Article

Desmin Mutation in the C-Terminal Domain Impairs Traction Force Generation in Myoblasts

Elisabeth E. Charrier,[1,2] Atef Asnacios,[2] Rachel Milloud,[3] Richard De Mets,[3] Martial Balland,[3] Florence Delort,[1] Olivier Cardoso,[2] Patrick Vicart,[1] Sabrina Batonnet-Pichon,[1] and Sylvie Hénon[2,*]

[1]Unité de Biologie Fonctionnelle et Adaptative, Université Paris Diderot, Sorbonne Paris Cité, CNRS, UMR 8251, Paris, France; [2]Matière et Systèmes Complexes, Université Paris Diderot, Sorbonne Paris Cité, CNRS, UMR 7057, Paris, France; and [3]LIPhy Université Grenoble 1, CNRS, UMR 5588, Grenoble, France

ABSTRACT The cytoskeleton plays a key role in the ability of cells to both resist mechanical stress and generate force, but the precise involvement of intermediate filaments in these processes remains unclear. We focus here on desmin, a type III intermediate filament, which is specifically expressed in muscle cells and serves as a skeletal muscle differentiation marker. By using several complementary experimental techniques, we have investigated the impact of overexpressing desmin and expressing a mutant desmin on the passive and active mechanical properties of C2C12 myoblasts. We first show that the overexpression of wild-type-desmin increases the overall rigidity of the cells, whereas the expression of a mutated E413K desmin does not. This mutation in the desmin gene is one of those leading to desminopathies, a subgroup of myopathies associated with progressive muscular weakness that are characterized by the presence of desmin aggregates and a disorganization of sarcomeres. We show that the expression of this mutant desmin in C2C12 myoblasts induces desmin network disorganization, desmin aggregate formation, and a small decrease in the number and total length of stress fibers. We finally demonstrate that expression of the E413K mutant desmin also alters the traction forces generation of single myoblasts lacking organized sarcomeres.

INTRODUCTION

The cytoskeleton plays a central role in mechanobiology by transmitting mechanical and chemical stimuli within and between cells. It provides organization and structure within the cytoplasm, and dictates the viscoelastic and mechanical properties of cells. It also controls many dynamic processes, such as intracellular trafficking, cell division, and adhesion, mainly through interactions with molecular motors. The cytoskeleton is a complex network of microfilaments, microtubules, and intermediate filaments (IFs). Until recently, most studies of cell mechanics were dedicated to the role of actin filaments and microtubules. However, several recent studies suggest a key role of IFs in determining viscoelastic properties of cells (1,2) in addition to mechanosensing (3–5). Still, the precise roles of IFs in cells mechanical properties remain less clear than for other cytoskeletal proteins, even though they are expressed in most differentiated cells.

The IF family is composed of five subtypes. These fibrous proteins harbor a common tripartite organization, characterized by a central α-helical coiled-coil-forming domain and non-α-helical head and tail domains of variable length and sequence (6). Except for lamins (type V IF), which are nuclear and universally expressed in higher eukaryotes, IFs are cytoplasmic and exhibit tissue-specific expression. Our study focuses on desmin, a type III IF specifically expressed in muscle cells and frequently used as a skeletal muscle differentiation marker.

Most of the previous studies concerning type III IF have focused on vimentin, an IF expressed by fibroblasts that has a strong sequence homology with desmin. The vimentin IF network plays a role in mechanosensing through focal adhesions (3,4,7,8) and modulates the viscoelasticity of cells during large deformation (9,10). However, the effect of desmin on the mechanical properties of cells is much less documented.

Desmin is mostly studied in a pathological context. Around sixty mutations in desmin human gene that can lead to desminopathies have been reported up to date. Desminopathies constitute a subgroup of myofibrillar myopathies leading to restrictive or dilated cardiomyopathies frequently associated with progressive skeletal weaknesses (11). Patient's skeletal muscles are histologically characterized by the presence of protein aggregates containing desmin, associated with a disorganization of the contractile apparatus (12,13). To date, desmin mutations have been mostly studied using either in vitro polymerization experiments or murine models (14–19). In vitro experiments have shown that desmin mutants have impaired abilities to form filaments, and that the mechanical properties of individual filaments or solutions of filaments were also affected (14–17,20).

Only a few studies have investigated the consequences of mutant desmin expression on the viscoelasticity of

Submitted June 12, 2015, and accepted for publication November 23, 2015.

*Correspondence: sylvie.henon@univ-paris-diderot.fr

Editor: David Piston.

0006-3495/16/01/0470/11

http://dx.doi.org/10.1016/j.bpj.2015.11.3518

myoblasts (21,22). We have recently shown that a specific desmin mutant affects the dynamics of cell reorientation in response to cyclic stretch (23). But the impact of desmin mutation on force generation by isolated cells has yet to be investigated.

In this study, we measured both the passive mechanical properties and active force generation of myoblasts exhibiting the E413K mutation of the desmin gene. This mutation is implicated in myofibrillar myopathy. It is located in the C-terminal domain and leads to protein aggregation, associated with a disorganization of the desmin network and severe muscle weakness in patients (24). Among the different mutated desmin mutants that we tested (25,26), we focus here on the E413K desmin. When expressed in myoblasts, it gives both a network and small desmin aggregates that do not constrain the nucleus, contrary to large aggregates observed with other mutants (25,26).

In this study we used C2C12 myoblasts either only expressing endogenously functional desmin or electroporated with wild-type (WT) or mutant desmin. We studied the organization of the desmin and actin networks in three cell types: nonelectroporated C2C12 myoblasts, C2C12 expressing an exogenous WT desmin fused with green fluorescent protein (GFP), and C2C12 expressing E413K-mutated desmin fused with GFP. We also characterized both the passive and active mechanical properties of these cells. On the one hand, using a custom-designed single cell rheometer (SCR) (parallel plates), we characterized the viscoelastic properties of cells by measuring their overall creep properties; on the other hand, traction forces developed by isolated cells were measured using two techniques, single cell rheometry and traction force microscopy (TFM).

MATERIALS AND METHODS

Plasmids

The complete human desmin WT cDNA from a previously generated pLink vector (25,26) was subcloned in a pEGFP-C1 plasmid with an *Eco*RI-XbaI restriction site. Single nucleotide mutations in the desmin sequence were obtained using the QuickChange II Site-Directed Mutagenesis Kit (Agilent New Technologies, Santa Clara, CA) according to the manufacturer's instructions. These desmin mutations are similar to those observed in patients with desminopathies. The constructs named pEGFP-des-WT or pEGFP-Des-mut allow production of WT or mutated desmin E413K fused with an N-terminal GFP tag. All desmin sequences were verified by sequencing (Eurofins, MWG, Ebersberg, Germany).

Cell line, culture, and electroporation

C2C12 cells (ATCC) were grown in Dulbecco's modified Eagle's medium (DMEM, Life Technologies) supplemented with 10% fetal bovine serum (PAA Laboratories, Pasching, Austria) and 1% penicillin/streptomycin (Life Technologies, Carlsbad, CA). pEGFP constructs were electroporated in C2C12 cells using a Gene Pulser II (BioRad, Hercules, CA). Briefly, cells were trypsinized (Trypsin-EDTA, Life Technologies) 5 min at 37°C and resuspended in complete DMEM medium at 2×10^6 cells/mL. 400 μL of the cell suspension were then introduced in a Gene Pulser Cuvette 0.4 cm (BioRad) and submitted to 250V, 1 mF during ~25 ms. After electroporation, cells were plated on glass coverslips (VWR International, Radnor, PA) 24 h before confocal microscopy or optical tweezers experiments. For SCR, 24 h after electroporation cells were detached from the culture dish using trypsin-EDTA, resuspended in medium, and left under weak agitation for 2 h before experiment. All the experiments were performed in DMEM medium without phenol red complemented with 10% fetal bovine serum, 1% penicillin/streptomycin, and 0,15% HEPES.

Micropatterns

The procedure has been described elsewhere (27). Briefly, poly(*N*-isopropylacrylamide) brushes were grafted on glass coverslips, except on regions that were devoid from polymerization initiator by illumination with deep ultraviolet through synthetic quartz/chromium masks with desired features. These regions were functionalized with fibronectin and seeded with cells for 2 h. The patterns used here were squares with an area of 900 μm^2, adapted to ensure full spreading of cells on each pattern in the area (27).

Immunostaining and confocal microscopy

Cells were fixed 24 h after electroporation and 2 h after seeding for experiments on micropatterns with 2% paraformaldehyde (Affymetrix) for 15 min at room temperature (RT) and permeabilized 5 min with 0.5% Triton X-100. DNA was stained with Hoechst 1 μg/mL (Sigma-Aldrich, St. Louis, MO) for 10 min at RT. Actin was stained with phalloidin coupled to Alexa fluor 647 (Life Technologies) at 1:250 for 30 min at RT. Immunofluorescence staining of desmin was performed as follows: fixed and permeabilized cells were incubated with serum albumin bovine at 1 μg/mL for 20 min. Desmin was then stained using rabbit polyclonal antidesmin antibodies (Biogenesis, Poole, UK) at 1:50 diluted in phosphate buffered saline (PBS), for 1 h at RT. Vimentin was stained with the same procedure using antivimentin at 1:500 (Ab-Cam, Cambridge, UK). Secondary antirabbit AlexaFluor488 antibodies (Life Technologies) were added at 1:1000 for 1 h at RT. Detection of Myc-desmin in C2C12 cells was performed in similar conditions, using anti-Myc antibody (9E10, Santa Cruz Biotech, Dallas, TX) at 1:100. Finally, cells were rinsed three times in PBS and mounted with Fluoromount medium (Interchim). Images were taken with a confocal microscope (Zeiss LSM 700, Oberkochen, Germany). Aggregation rates of desmin-GFP in myoblasts were evaluated by taking at least three separate 5×5 tile scan images (corresponding to 25 pictures) chosen randomly in fields containing Hoechst-stained areas. Nuclei and cells containing GFP fluorescence associated or not with aggregates were visualized on images and manually counted. We determined the electroporation rate in the population by calculating the ratio between the number of fluorescent cells and the number of nuclei. Finally, we calculated the aggregation rate as the ratio between the number of cells containing aggregates and the number of cells expressing GFP.

Image analysis

Segmentation and analysis of cell stress fibers was carried out using a custom plug-in and various macros written for Fiji (28). The procedure is very similar to the one described in (29) and is fully explained in the Supporting Material.

Western blot analysis

24 h after electroporation culture dishes containing cells were washed three times in PBS and proteins were extracted with RIPA buffer (50 mM Tris, 150 mM NaCl, 1% NP40, 5 mM EDTA, 1 mM NA_3VO_4, 10 mM NaF, PMSF 1 mM, and antiprotease mix from Sigma-Aldrich). Proteins were separated by sodium dodecyl sulfate polyacrylamide gel

electrophoresis (SDS-PAGE) electrophoresis on a 10% acrylamid-bisacrylamide gel and transferred to nitrocellulose membranes (Macherey Nagel, Duren, Germany). Membranes were saturated with 5% milk in PBS 0.5% Tween. Primary antibodies were then added: Rabbit polyclonal antidesmin (Biogenesis England, Biotechnologies) at 1:250, mouse monoclonal anti-α-actin (clone 4, Merck Millipore, Darmstadt, Germany) at 1:2000, rabbit monoclonal antivimentin at 1:5000 (AbCam), rabbit polyclonal anti-glyceraldehyde-3-phosphate dehydrogenase (GAPDH) (Sigma-Aldrich) at 1:15000, or rabbit polyclonal anti-GFP (Life Technologies) at 1:3000. Isotype-specific secondary antibodies coupled with a horseradish peroxydase (Pierce) were then added at 1:10000 and revealed by incubating the membrane with enhanced chemiluminescence (Pierce, Waltham, MA). A charge-coupled device camera FUJI Las 4000 (GE Healthcare, Little Chalfont, UK) was used to take pictures of the membrane.

SCR

Creep function measurements

We used a custom-made uniaxial stretching device (30,31) to globally deform cells and measure their creep function. Briefly, cells were trypsinized and centrifugated at 140 × *g* for 3 min, diluted in DMEM supplemented with 15 mM HEPES, and maintained under smooth agitation for 2 h at 37°C. The delay of 2 h was necessary for the cells to regenerate adhesion proteins expressed at the cell surface. The experimental chamber was filled with this cell suspension, and a cell was caught between two parallel glass microplates coated with fibronectin (32), as schematically depicted in Fig. 1. One plate was rigid, the other one flexible and used as a spring of calibrated stiffness k. After waiting for 2–3 min to allow cell spreading on the microplates, a controlled deflection δ was applied to the flexible microplate and held constant in time via a feedback loop (31). This allowed us to apply a controlled constant traction force on the cell, $F = k\delta$, and thus a constant stress $\sigma_0 = F/S = k\delta/(\pi R^2)$, where R is the apparent contact radius between the cell and the plates, measured from bright field images. We assume that cell/plates contact areas are disks, the diameters of which can be measured from lateral view images (33) (see Fig. S1). The cell strain $\varepsilon(t)$ was calculated from the measured cell length $L(t)$ and its initial value L_0: $\varepsilon(t) = (L(t)\text{-}L_0)/L_0$. The creep function was then assessed using the relationship: $J(t) = \varepsilon(t)/\sigma_0$. The cell strain was always smaller than 10% to ensure a linear deformation regime.

Characterizing traction force generation by a single myoblast

The same setup also allows one to measure the force generated by an isolated cell. A single myoblast spreading between the two parallel plates exerts forces that deflect the flexible microplate (32,34). The force generated as a function of time can be retrieved from the deflection $\delta(t)$ of the flexible microplate of stiffness k: $F(t) = k\,\delta(t)$. After measuring the creep function of an isolated cell over a period of typically 10 s, the cell was relaxed to its original length L_0. The setup was then switched to a constant length mode (isometric traction), in which a feedback loop adapts the flexible plate deflection to counteract the force generated by the cell. We have previously shown that these conditions lead to maximum values of the rate of force increase dF/dt as well as of the plateau traction force F_p (31,34). These experiments, where the distance between the parallel microplates is maintained constant in time, are similar to isometric exercise of a muscle, in which the muscle develops its maximum force by contracting without changing length. We measured the rate of force build-up, $dF/dt = k\,d\delta/dt$, in these conditions.

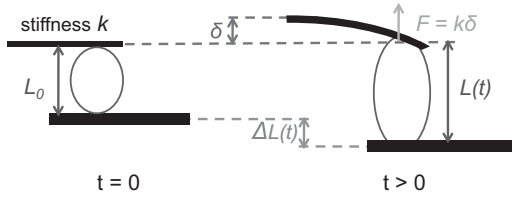

FIGURE 1 Schematic drawing of a creep experiment with the SCR. A cell is caught between a flexible microplate with a stiffness k (*top*) and a rigid one (*bottom*), with an initial length L_0. At $t = 0$ the flexible microplate is deflected by δ, and this deflection is then maintained constant over time by a feedback loop applying a displacement $\Delta L(t)$ to the rigid microplate. The constant applied stress is inferred from the constant deflection δ, whereas the cell deformation is retrieved from its elongation $\Delta L(t)$.

TFM

TFM experiments were performed to quantify the contractile energy transmitted by cells to a 5 kPa polyacrylamide gel substrate. The experimental procedure is described in detail in (35). Briefly, acrylamide and bisacrylamide solutions were mixed (ratio 37.5:1) in Dulbecco's phosphate buffered saline (Gibco, Waltham, MA) at 6.7% final concentration. Fluorescent far red beads (dark red 200 nm, Invitrogen F-8807, Waltham, MA) were dispersed in this solution by sonication, and 1 μL *N*,*N*,*N*′,*N*′-tetramethylethyliendiamine and 1 μL ammonium persulfate were finally added. A droplet of this solution was plated between two coverslips, one of which had been silanized with 3-(trimethoxysilyl)-propyl methacrylate. After polymerization gel was detached from the nonsilanized coverslip and incubated during 30 min in a *N*-hydroxysuccinimide (Sigma) and *N*-(3-dimethylaminopropyl)-*N*-ethylcarbodiimide hydrochloride (Sigma) solution. Finally, the gel was coated with a 30 μg/mL fibronectin solution (Sigma) during 1 h at 37.5°C. Cells were plated on the gel 24 h after electroporation and incubated for 2 h before starting experiments. Coverslip was mounted in a chamber under an inverted microscope (Ti-E; Nikon (Tokyo, Japan), 63X air objective, NA 1.4) equipped with a charge-coupled device camera (CoolSNAP; Roper Scientific, Trenton, NJ) and maintained at 37°C. The deformation field of the gel was assessed from beads displacements analysis determined from fluorescence images before and after removal of cells with trypsin. Quantification of traction stresses exerted by cells on the substrate was extracted from gel strain by using the Fourier-transform traction cytometry method (36,37).

Statistics

Distributions of the different measured values were tested using Shapiro-Wilk tests for their normality. Because most values do not exhibit normal (Gaussian) distributions, adapted nonparametric tests were performed. Tests were performed using a statistical significance level of 5%.

RESULTS

All experiments were performed on three cell types: nonelectroporated C2C12 cells (C2C12-NE), C2C12 expressing WT human desmin fused with GFP (C2C12-WT-GFP), and C2C12 expressing E413K mutated human desmin fused with GFP (C2C12-E413K-GFP). C2C12-WT-GFP served as controls for our investigation of the influence of overexpression of WT desmin and its fusion with GFP on the morphology of the desmin network and on the cells mechanical properties. C2C12-E413K-GFP are cellular models for desminopathies with a simultaneous expression of endogenous WT desmin and exogenous mutated desmin. GFP-tag was used to recognize cells expressing exogenous desmin.

Exogenous desmin is expressed at a physiological level in electroporated myoblasts and induces no change in actin expression nor in vimentin expression

Expression profiles were quantified by Western blot WB analysis on at least three independent WB, using GAPDH expression level as a reference. The amount of endogenous desmin is unchanged by the electroporation process: electroporated myoblasts expressed as many endogenous desmin as C2C12-NE. Furthermore, a moderate amount of exogenous desmins were overexpressed in electroporated cells as compared to endogenous (Table 1). Indeed, C2C12-WT-GFP cells express on average 1.9 molecules of exogenous desmin per endogenous desmin, whereas for C2C12-E413K-GFP cells the ratio is 2.0/1 (Table 1 and Fig. 2, *A* and *B*). Moreover, we have verified that GFP is not cleaved from exogenous desmin, which would lead to a bias in the calculation of the exogenous to endogenous desmin ratio (Fig. S2). We also investigated whether desmin overexpression had an impact on the expression of actin, which plays a central role in cell mechanics and dynamics. Using GAPDH as a reference (Fig. 2 *A*) we measured that the actin expression level was not disturbed in cells expressing desmin-WT-GFP or mutant desmin-E413K-GFP. Finally, we investigated whether desmin overexpression alters vimentin expression. Vimentin expression in myoblasts is downregulated during myogenesis in favor of desmin upregulation. Using GAPDH as a reference (Fig. 3, *A* and *B*), we measured that the vimentin expression level was not disturbed in desmin-WT-GFP or mutant desmin-E413K-GFP as compared to nonelectroporated (NE) cells.

Expression of E413K mutated desmin disturbs the desmin network morphology, but not the vimentin network, and decreases the number and length of stress fibers

The endogenous desmin network of immunostained C2C12-NE cells was imaged in confocal microscopy. Cells show well individualized and interconnected desmin filaments (Fig. 2 *C*). The desmin network is cytoplasmic, spreading from nucleus to cell membrane with a higher density around the nucleus. The actin network is mostly located at the cell periphery and in stress fibers.

TABLE 1 Quantification of Exogenous to Endogenous Desmin Ratios

	C2C12-WT-GFP	C2C12-E413K-GFP
Fraction of GFP positive cells (electroporation rate)	44%	40%
Exogenous to endogenous desmin ratio from western blot analysis	0.9 ± 0.1	0.8 ± 0.1
Normalized exogenous to endogenous desmin ratio	1.9 ± 0.2	2.0 ± 0.1

C2C12-E413K-GFP cells show two phenotypes: 70% of the cells display a regular desmin network, whereas ~30% contain both a network and aggregates containing desmin (Fig. 2 *D*). Aggregates vary in number, morphology, and location within cells. Most cells containing aggregates display multiple aggregates that are typically smaller than 0.5 μm in diameter and randomly distributed all over the cytoplasm. However, some cells show a single large aggregate often located at the nucleus periphery. Most of the C2C12-WT-GFP cells exhibit healthy desmin network morphology, yet 8% of the cells still contain cytoplasmic aggregates of desmin-WT-GFP. This aggregation is presumably due to the fusion with the GFP tag in the N-terminal end of desmin, which leads to a ubiquitous increase of aggregation.

We also checked if endogenous and mutated desmin could colocalize by using C2C12 cells coexpressing desmin-WT-Myc and desmin-E413K-GFP. We evidence a colocalization of the two desmin cytoplasmic networks (Fig. S3). Furthermore, desmin-WT-Myc is also found in aggregates rich in desmin-E413K-GFP (Fig. S3). Desmin-WT-Myc is visible as a ring at the periphery of the largest aggregates, presumably because the antibody is unable to diffuse inside this dense structure.

The vimentin network of immunostained C2C12 cells was similarly imaged in confocal microscopy for the three cell types. As desmin and vimentin can copolymerize in vitro, we checked whether vimentin distribution was altered by the expression of exogenous desmin. The vimentin network is cytoplasmic, spreading from nucleus to cell membrane with a lower density around the nucleus in all cases (Fig. 2 *E*). Neither WT-desmin-GFP nor mutant desmin-E413K-GFP expression induces vimentin aggregation or alteration of its localization, even in the presence of aggregates (Fig. 2 *E*).

The actin network was also imaged in the three cell lines, using Alexa fluor 647 phalloidin. It shows a healthy morphology in all cell lines (Fig. 2, *C* and *D*), in both its distribution as well as in the formation of stress fibers. The presence of desmin aggregates, including large ones, does not disrupt the actin network and we found no detectable colocalization of actin with the aggregates. We measured the areas and shape factors for the three cell types and found no significant differences, although there is a slight shift in the area distribution toward large values for C2C12-WT-GFP cells.

A detailed analysis of stress fibers distribution showed small but significant differences for the myoblasts expressing the desmin E413K mutant. This difference was quantified using cells plated on adhesive micropatterns, to decouple the effect of desmin mutation on the stress fibers distribution from the cells size and shape variability. The cells were constrained to an adhesive square micropattern (Fig. 3). The stress fibers were automatically detected on the fluorescence images, following the procedure described

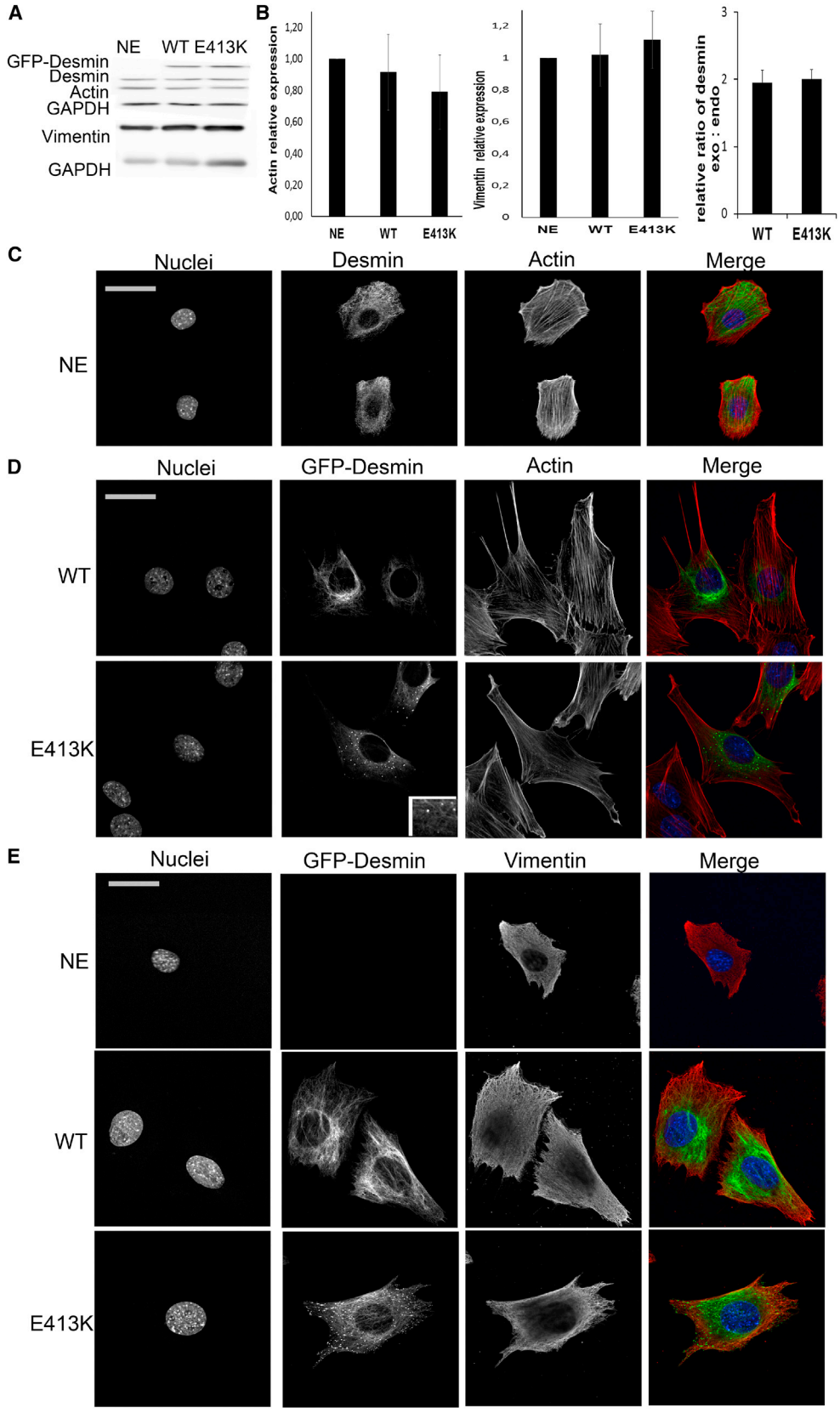

FIGURE 2 Impact of desmin-GFP expression on the cells cytoskeleton. (*A*) Typical immunoblots for analyzing desmin, actin, and vimentin contents in nonelectroporated C2C12 cells (NE), C2C12 expressing WT desmin-GFP or E413K mutated desmin-GFP (E413K). GAPDH is used as a loading control.

(legend continued on next page)

in the Material and Methods and Supporting Materials and Methods sections. Their number, lengths, and orientation with respect to the cells large axis (diagonal of the square) were measured for each cell. There were no significant differences in the orientation of the stress fibers in the three cell lines. On the contrary, both the number and mean length of the stress fibers were significantly smaller for myoblasts expressing the E413K desmin mutant. The results are summarized in Table 2 and Fig. 3 *B*. Altogether, the total length of stress fibers is ~25% smaller in C2C12-E413K-GFP than in the two other cell lines. There were no significant differences between cells with or without desmin aggregates.

Overexpression of WT desmin increases cell rigidity

A typical measurement of cell creep function $J(t)$ as measured with the SCR is displayed in Fig. 4 in log-log scale. As already observed (38–40), $J(t)$ can be fitted by a power law of time (Fig. 4), $J(t) = At^{\alpha}$, over more than two decades, 0.1s–10s, for all cell types. As previously discussed (39), this is equivalent to a viscoelastic modulus G varying as a power-law of frequency f ($G = G_0 f^{\alpha}$, $G_0 = (2\pi)^{\alpha}/[A\Gamma(1 + \alpha)]$), and a constant phase-shift, $\tan(\alpha\pi/2)$, between the storage (elastic) part G' and the loss (viscous) part G'' of G: G_0 is a measure of the cell rigidity at 1 Hz and α is a measure of the repartition between elasticity and viscosity into the cell.

For the three cell-types characterized in this study, values of α show approximately normal (=Gaussian) distributions, whereas values of G_0 show broad approximately log-normal distributions (Fig. 5): the cumulative distributions of α and of $\log(G_0)$ roughly show the characteristic shape of error functions. These results are consistent with previous measurements (30,39,40). The measured mean values of α and geometric mean values of G_0 are displayed in Table 3. The values of α as measured with the SCR show very similar distributions for the three cell types, with a mean value of 0.22 for C2C12-NE and C2C12-E413K-GFP cells, and of 0.20 for C2C12-WT-GFP cells. This slight difference is just beyond significance.

In contrast, the measured geometric mean value of G_0 is higher for C2C12-WT-GFP than for other cell types: the expression of desmin-WT-GFP significantly increases the rigidity of the cells from ~400 Pa to ~600 Pa. We thus observe a significant increase in cell rigidity when functional desmin is added in myoblasts. On the contrary, such an increase is not observed with the expression of mutated E413K desmin.

Expression of E413K mutated desmin decreases the rate of force generation of single myoblasts in three-dimensional geometry

Combined measurements of creep function and rate of force generation

After the creep measurement, the cell is relaxed to its initial length. The setup is then switched to a mode allowing the cell to deflect the flexible plate while spreading. In these conditions, the cell generates a force increasing linearly with time after typically 1 min transient regime ((32) and Fig. S4). This phase of constant rate of force production lasts for 10 to 40 min, and the force finally saturates to a plateau value ((32) and Fig. S4). The values of the plateau force F_p and the rate of force generation dF/dt are correlated (32). We have previously shown that dF/dt increases with the stiffness k of the plate the cell is pulling on, and saturates at a maximum value for infinite stiffness, just as F_p does (32,34). In this work, using the infinite stiffness mode of the SCR (see Materials and Methods section for details), we have measured this maximum value of dF/dt and we use it as a measure of the ability of the cell to generate traction forces. dF/dt was measured for each cell through a linear fit of the $F(t)$ curve on a typical time range of 10–20 min (Fig. S4).

The rate of force generation is reduced by desmin mutation and aggregation

The measured values of dF/dt show wide distributions for all cell types. These distributions are approximately log-normal for both control C2C12-NE cells and C2C12-WT-GFP cells: The cumulative distributions of $\log(dF/dt)$ roughly show the characteristic shape of error functions (Fig. 6). The geometrical mean value of dF/dt is ~80 pN/s for the two cell types. For C2C12-E413K-GFP cells on the contrary, the distribution of dF/dt is clearly not log-normal, with a spreading in the low values domain. To

Actin expression is similar in the three cell types. (*B*) Quantification of actin, vimentin, and desmin expression levels, normalized by GAPDH. The control value obtained with NE cells is used as a reference. Actin and vimentin expressions are unaltered by overexpressing WT- or E413K-desmin-GFP. The two desmin-GFP constructs are moderately overexpressed, without impact on the level of endogenous desmin. All these quantifications have been made on five (desmin) or four (actin and vimentin) independent electroporation experiments. (*C*) Confocal images of actin and desmin in C2C12-NE cells. Desmin is stained by immunofluorescence, actin is stained with phalloidin, and nuclei with Hoechst. Scale bar = 20 μm. (*D*) Confocal images of actin and desmin in C2C12-WT-GFP cells and C2C12- E413K-GFP cells. Desmin is directly visualized by imaging the GFP. C2C12-WT myoblasts exhibit a normal desmin network. C2C12-E413K cells display two phenotypes: 70% of cells contain only a desmin network, 30% of cells contain both a desmin network and cytoplasmic aggregates, which can be clearly seen on the enlarged box (X3). The actin network shows a healthy morphology for the two cell types. Scale bar = 20 μm. (*E*) Confocal images of vimentin and desmin in NE, C2C12-WT-GFP, and C2C12- E413K-GFP cells. Vimentin is immunostained and exogenous desmin is directly visualized by the GFP. C2C12-WT-GFP and C2C12-E413K-GFP cells exhibit a normal vimentin network, even in cells containing cytoplasmic desmin aggregates, without colocalization in desmin aggregates. Scale bar = 20 μm

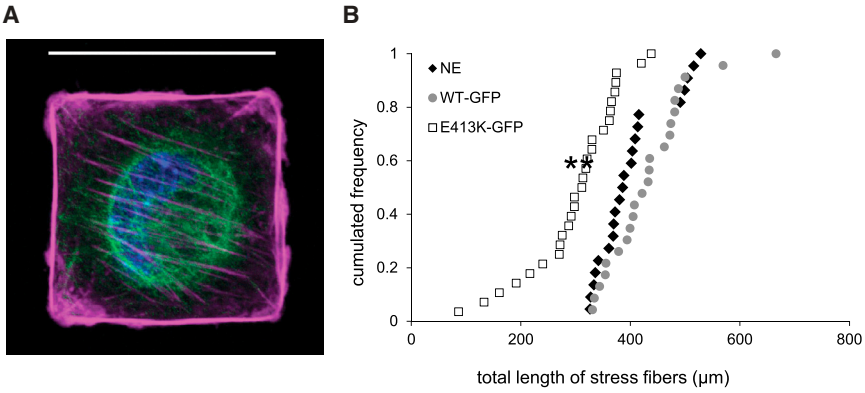

FIGURE 3 (*A*) C2C12-WT-GFP myoblast on an adhesive fibronectin micropattern; the nucleus appears in blue, WT-desmin-GFP in green, and actin fibers in magenta. Scale bar = 30 μm. (*B*) Cumulative distributions of the total length of stress fibers per cell, for single C2C12-NE (NE), C2C12-WT-GFP (WT), and C2C12-E413K-GFP (E413K) on square adhesive micropatterns. The stars symbol indicates significant *p*-value ($p < 0.01$) for C2C12-E413K-GFP cells.

elucidate the origin of this modified distribution, C2C12-E413K-GFP cells were separated in two subgroups: cells containing cytoplasmic desmin aggregates (+) and those without aggregates (−). Indeed, the two subgroups show distinct contractile properties: C2C12-E413K-GFP cells without cytoplasmic aggregates show *dF/dt* values similar to control cells (C2C12-NE and C2C12-WT-GFP), whereas C2C12-E413K-GFP cells containing cytoplasmic aggregates display significantly lower values of *dF/dt*, by ~fourfold (Fig. 6 and Table 4). We checked whether this decrease in force generation was solely due to the presence of desmin aggregates, by similarly separating C2C12-WT-GFP cells in two subgroups: those containing desmin aggregates (+) and those without aggregates (−). The distributions of *dF/dt* values are similar for the two subgroups (Fig. 6 and Table 4). Note that to obtain relevant statistics, experiments were performed on a large number of C2C12-WT-GFP + cells, which is not representative of the percentage of aggregates positive cells in the C2C12-WT-GFP population.

Fig. 6 and Table 4 summarize the results obtained on the five groups and subgroups of C2C12 cells: The values of *dF/dt* show approximately log-normal distribution for all cell types. All cell types have similar distributions and geometric mean values of *dF/dt*, except C2C12-E413K-GFP+ cells, which show a large decrease in the *dF/dt* value, by fourfold. In contrast C2C12-WT-GFP+ cells do not show this decrease in force generation.

We checked that this difference was not due to a difference in the spreading velocity of cells on microplates: it does not significantly differ for the different cell types and is equal to 6 nm/s on average.

TABLE 2 Properties of the Stress Fibers for the Three Cell Types on Square Micropatterns

	No. of Stress Fibers per Cell	Mean Length of Stress Fibers (μm)	Total Length of Stress Fibers per Cell (μm)
C2C12-NE	75 ± 8	5.4 ± 0.6	403 ± 47
C2C12-WT-GFP	81 ± 13	5.4 ± 0.6	436 ± 61
C2C12-E413K-GFP	63 ± 12	4.8 ± 0.7	298 ± 58

We finally checked whether cell aggregates could be a consequence rather than a cause of the observed smaller rate of force generation, by measuring the percentage of C2C12-E413K-GFP cells that show cytoplasmic aggregates when they are treated with 5 or 15 μM of blebbistatin. This drug decreases the contractility of cells and has been shown to decrease the level of forces generated by myoblasts in the SCR (32). Cells were treated 8 h after electroporation with blebbistatin (Sigma) 5 or 15 μM overnight and then fixed and immunostained. We measured no significant influence of blebbistatin on the aggregation rate in C2C12-E413K-GFP cells.

Mutated desmin impairs myoblasts contractile energy in two-dimensional geometry

We tested if a decrease in myoblast force generation ability induced by mutated desmin expression was also observed in a more traditional two-dimensional (2D) cell-culture-like geometry by performing TFM measurements. Such experiments allow one to measure the contractile energy *Ec* spent by adherent cells to deform their substrate. Fig. 7 and Table 5 display the results obtained on the different cell types. C2C12-NE cells and C2C12-WT-GFP cells show comparable distributions of *Ec*, with a geometric mean value of ~8.5 10^{-15} J, whereas C2C12-E413K-GFP cells develop a much smaller *Ec*, with an average value of ~3.5 10^{-15} J.

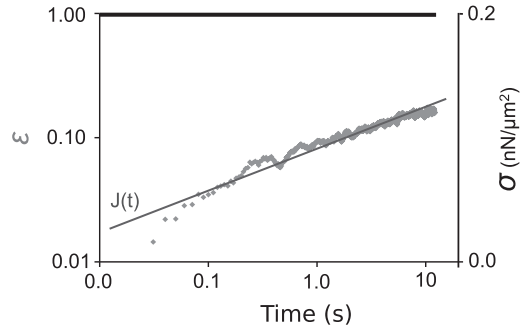

FIGURE 4 Creep experiment carried out with the SCR. The cell strain ε under constant applied stress is plotted as a function of time in log-log scale. ε is well fitted by a power law of time, over two decades.

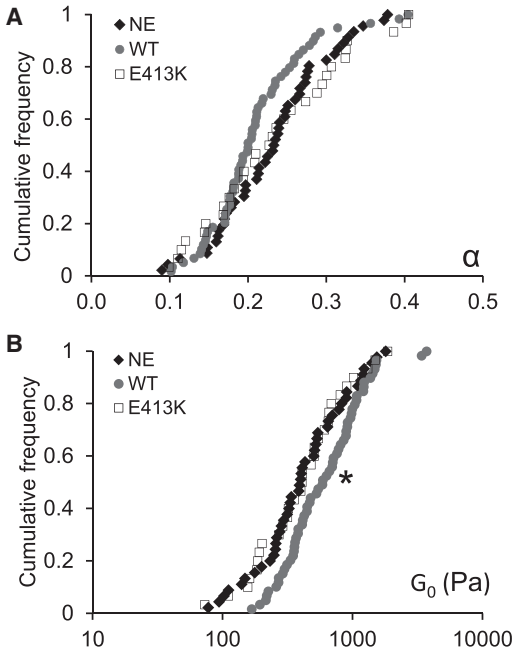

FIGURE 5 Cumulative distributions of α values (*A*) and of G_0 values (*B*), for single C2C12-NE (NE, $n = 43$ cells), C2C12-WT-GFP (WT, $n = 60$ cells), and C2C12-E413K-GFP cells (E413K, $n = 30$ cells). There are no significant differences in α values between the three cell types. The star symbol indicates a significant *p*-value ($p < 0.05$) for C2C12-WT-GFP cells, which are stiffer than the two other cell types.

Both aggregate positive and aggregate negative cells expressing E413K mutated desmin show a drop down of *Ec* by ~threefold as compared to control cells. Strikingly, the loss in contractile energy is in the same order of magnitude as the loss in the rate of force generation in SCR experiments.

DISCUSSION

In this work, we have used an isogenic model, C2C12 cells electroporated with plasmids coding for WT or mutant desmin, to study the effect of a desmin overexpression and a desmin mutation on cytoskeleton organization and on cell passive and active mechanical properties at a very short time after expression. Using electroporation instead of lipofection allowed us to obtain moderate overexpression levels of exogenous desmin. We show that exogenous WT desmin fused with GFP is able to polymerize within the cytoplasm

TABLE 3 Values of G_0 and α for the Three Cell Types

	G_0 Values (Pa)		
	Geometric Mean Values	Confidence Interval	α Values
C2C12-NE	408	187 to 891	0.22 ± 0.01
C2C12-WT-GFP	603	305 to 1189	0.20 ± 0.01
C2C12-E413K-GFP	405	186 to 881	0.22 ± 0.01

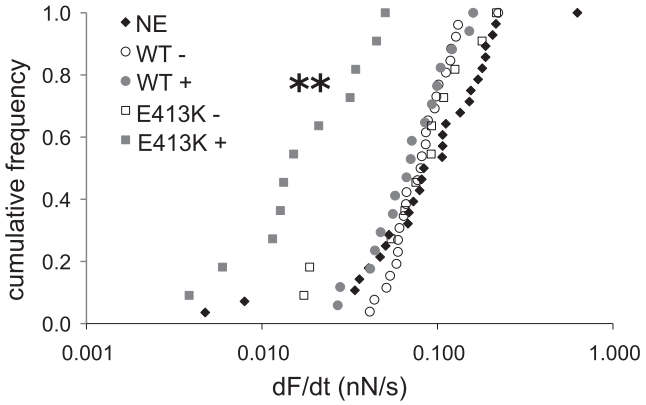

FIGURE 6 Cumulative distributions of the rate of force generation *dF/dt* as measured with the SCR for single C2C12-NE (NE, $n = 28$ cells), C2C12-WT-GFP and C2C12-E413K-GFP cells. Both C2C12-WT-GFP and C2C12-E413K-GFP populations are divided into two subpopulations: "–" containing only desmin network (WT –, $n = 26$ cells, and E413K –, $n = 11$ cells), and "+" containing both aggregates and network of desmin (WT +, $n = 17$ cells, and E413K +, $n = 11$ cells). The distribution for E413K+ cells is shifted toward small values in comparison to other cell types ($p < 0.01$).

and induces a 1.5-fold increase in the global rigidity of myoblasts. This is consistent with results obtained on the role of vimentin in the mechanical properties of fibroblasts (1,10). Vimentin is a type III IF, homologous to desmin, and is also expressed in connective tissues and in immature myoblasts. It was shown that the lack of vimentin expression induces a twofold decrease in the elastic modulus of fibroblasts' cytoplasm (1,10). Similarly, the increase in the viscoelastic modulus that we measured here for C2C12-WT-GFP cells could be due to an increase in the stiffness of the cytoplasm in cells overexpressing WT desmin. Strikingly, this effect is not observed with the desmin-E413K-GFP mutant. It has been previously reported that desmin-E413K is unable to form filaments in vitro (41), presumably because its tetramers are hyper stable, and that it does not copolymerize with WT desmin, neither in vitro nor in transfected C2C12 cells. Indeed, the mutation is located on the last amino acid of the highly conserved YRKLLEGEE motif of IFs, which has been shown to play a central role in the proper formation of tetramers (42). We observe here that, though inducing the formation of aggregates in 30% of the cells, desmin-E413K-GFP is able to polymerize in C2C12 cells, and probably to enter the endogenous desmin

TABLE 4 Values of the Rate of Force Generation, *dF/dt*

	dF/dt (pN/s)	
	Geometric Mean Values	Confidence Interval
C2C12-NE	83	31 to 222
C2C12-WT-GFP –	80	55 to 118
C2C12-WT-GFP +	69	40 to 116
C2C12-E413K-GFP –	74	33 to 168
C2C12-E413K-GFP +	17	8 to 39

–, without aggregates; +, with aggregates.

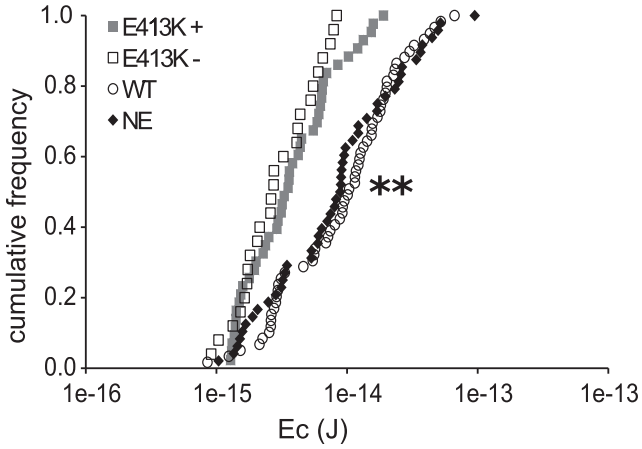

FIGURE 7 Cumulative distributions of the contractile energy E_c of single C212-NE (NE, $n = 48$ cells), C2C12-WT-GFP (WT, $n = 59$ cells), and C2C12-E413K-GFP cells as measured by TFM. C2C12-E413K-GFP population is divided into two subpopulations: "–" containing only desmin network and "+" containing both aggregates and network of desmin (E413K –, $n = 25$ cells, and E413K +, $n = 45$ cells). The statistics have been enriched in E413K + cells and is not representative of the repartition between "+" and "−" cells in the C2C12-E413K-GFP cells population. Cells expressing E413K mutated desmin, with or without cytoplasmic aggregates, show distributions of *Ec* values shifted toward low values in comparison to C2C12-NE and C2C12-WT-GFP cells ($p < 0.01$). The geometric mean value of E_c is three times lower for C2C12-E413K cells than for the two other cell types.

network. This polymerization is probably enabled by the low ratio of exogenous to endogenous desmins in electroporated cells (2:1), as compared to transfected cells (~10:1, data not shown). Yet the desmin-E413K-GFP network is unable to increase the viscoelastic modulus of the cell, contrary to desmin-WT-GFP. A possible interpretation of this result is that the mutated desmin shows a partial loss of function, preventing it to reinforce the endogenous desmin network. This is consistent with previous in vitro measurements, which have shown that the addition of most mutated desmins to WT desmin gels in vitro increases their viscosity, except for the E413K mutant (41). On the contrary, our results differ from the ones published on primary human myoblasts from patients with desminopathies, which appear stiffer than healthy ones (22). However, the two systems are fundamentally dissimilar. First, the mutations are of a different nature; second, the timescales of mutated desmin expression are different: endogenous expression for the primary myoblasts probably results in large remodeling in response to the expression of the mutated protein that was limited during the 24-h period used in our work. Additionally, primary myoblasts from healthy and desminopathy patients do not have the same genetic background, whereas in our work all cells are isogenic.

TABLE 5 Contractile energy values, as measured with TFM

	E_c (10^{-15} J)	
	Geometric Mean Value	Confidence Interval
C2C12-NE	8.2	2.7 to 25
C2C12-WT-GFP	9.0	3.3 to 25
C2C12-E413K-GFP −	2.9	1.5 to 5.6
C2C12-E413K-GFP +	3.7	1.7 to 8.0

−, without aggregates; +, with aggregates.

Because myoblasts generate traction forces and can contract their substrate, we have also characterized their force generation abilities. An important feature of the mechanical activity of the cells is the rate of force generation *dF/dt*, which is representative of the mechanical power, i.e., the energy per unit time invested by the cell to build up force and deform its mechanical environment (32). Using a single-cell parallel-plates setup (32,34), we quantified the mechanical activity of C2C12 cells by measuring the maximum *dF/dt* values in infinitely stiff conditions, similar to isometric contraction of muscles. We measured both the creep function $J(t)$ and the maximum rate of traction force generation *dF/dt* on each single tested cell. We could thus avoid any differences in the samples that may have hindered our comparison of the effects of desmin mutations on the passive and active features of myoblast mechanics. We observed that whereas the expression of desmin-WT-GFP increases the viscoelastic modulus of C2C12 cells, it has no effect on their ability to generate traction forces. Conversely, the expression of desmin E413K-GFP, which has no effect on the viscoelastic modulus of C2C12 cells, induces a fourfold decrease in their rate of force generation in the presence of aggregates. These disparate results for cells expressing two different desmins (WT-GFP vs. E413K-GFP) provide an internal control that the observed decrease in traction forces is neither due to GFP alone nor to overexpression of desmin alone. Using TFM to characterize the effect of desmin mutation on the traction forces generated by myoblasts in a more usual 2D substrate geometry, we also measured that the contractile energy of cells expressing desmin-E413K-GFP shows a threefold decrease as compared to NE cells or cells expressing desmin-WT-GFP. We thus demonstrate by two different techniques that E413K-mutation of desmin significantly decreases myoblasts abilities to generate traction forces. Nevertheless, the results obtained from rate of force generation (SCR) and from contractile energy measurements (TFM) slightly differ. TFM measurements, performed on cells spread for 2 h, show that the presence of the mutated desmin impairs the level of forces that C2C12 myoblasts develop and transmit to their substrate. This result is consistent with the observed reduced number and length of stress fibers in C2C12-E413K-GFP cells. The results are also in agreement with recent studies on vimentin: it was shown that the vimentin IF network, in fibroblasts and endothelial cells, is involved in the development of a high level of forces, in the maturation of focal adhesions, and more generally in mechanosensing through focal adhesions (3,5,7), presumably by regulating integrin functions. However, the mechanism underlying this effect

is not clear. On the other hand, with the SCR we measure the force generation rate of myoblasts in the first 10–20 min of spreading, presumably before the build-up of stress fibers. We show then that the build-up force of C2C12-E413K-GFP cells is affected only in the presence of desmin aggregates. One possible explanation for the difference between the two measurements could be that traction through cortical actomyosin at a short timescale, as measured with the SCR, is only affected when a large amount of functional desmin is trapped within aggregates, whereas long timescale traction forces (TFM) generated through stress fibers, involving more proteins of the cytoskeleton, could be altered even in cells presenting no aggregation.

CONCLUSIONS

We show that the desmin IF plays a role in both the passive and active mechanical properties of myoblasts. Until recently, little attention had been paid to dynamical properties of IFs and to their implication in force generation. The lack of research is likely because IFs are not associated with molecular motors like actin and microtubules. Our results, along with other recent works (3,43), highlight the implication of IFs in dynamical processes and active mechanical properties of cells. The cell-specific IF network is often pictured as an integrator of the actin and microtubules networks via a complex set of cross-bridging proteins (44), and thus could be involved in the actomyosin contractility by mechanisms that still have to be elucidated. Strikingly, E413K desmin mutation impairs stress fibers and force generation in myoblasts expressing mutated desmin for 24 h. This loss in tensile activity in the immature myoblast could play a role in the progressive muscle weakness observed in desminopathies, via the failure to establish a proper sarcomeric registry, which has been shown to alter contraction and calcium signaling in myocytes (45). This possible link and the related mechanisms will have to be explored in future experiments on myotubes.

SUPPORTING MATERIAL

Supporting Materials and Methods and eight figures are available at http://www.biophysj.org/biophysj/supplemental/S0006-3495(15)04702-5.

AUTHOR CONTRIBUTIONS

E.C. designed research, performed research, analyzed data, and wrote the article. R.M., R.D.M., and F.D. performed research. M.B. performed research and analyzed data. O.C. performed image analysis for stress fibers characterization. A.A., P.V., S.B.-P., and S.H. designed research, analyzed data, and wrote the article.

ACKNOWLEDGMENTS

The authors are indebted to P.A. Galie and J. Browaeys for careful reading of the manuscript and to the referees for their suggestions.

This work was supported by grants from Association Française contre les Myopathies (AFM 15454), Agence Nationale de la Recherche (ANR-13-BSV5-0017 and ANR-12-BSV5-0007-01), and Labex Who Am I? (transition postdoctoral program). Confocal pictures were performed at "plateau d'imagerie" of the BFA unit.

REFERENCES

1. Guo, M., A. J. Ehrlicher, …, D. A. Weitz. 2013. The role of vimentin intermediate filaments in cortical and cytoplasmic mechanics. *Biophys. J.* 105:1562–1568.
2. Mendez, M. G., D. Restle, and P. A. Janmey. 2014. Vimentin enhances cell elastic behavior and protects against compressive stress. *Biophys. J.* 107:314–323.
3. Lynch, C. D., A. M. Lazar, …, M. P. Sheetz. 2013. Endoplasmic spreading requires coalescence of vimentin intermediate filaments at force-bearing adhesions. *Mol. Biol. Cell.* 24:21–30.
4. Ivaska, J., H.-M. Pallari, …, J. E. Eriksson. 2007. Novel functions of vimentin in cell adhesion, migration, and signaling. *Exp. Cell Res.* 313:2050–2062.
5. Gregor, M., S. Osmanagic-Myers, …, G. Wiche. 2014. Mechanosensing through focal adhesion-anchored intermediate filaments. *FASEB J.* 28:715–729.
6. Strelkov, S. V., H. Herrmann, and U. Aebi. 2003. Molecular architecture of intermediate filaments. *Bioessays.* 25:243–251.
7. Tsuruta, D., and J. C. R. Jones. 2003. The vimentin cytoskeleton regulates focal contact size and adhesion of endothelial cells subjected to shear stress. *J. Cell Sci.* 116:4977–4984.
8. Mendez, M. G., S. Kojima, and R. D. Goldman. 2010. Vimentin induces changes in cell shape, motility, and adhesion during the epithelial to mesenchymal transition. *FASEB J.* 24:1838–1851.
9. Gladilin, E., P. Gonzalez, and R. Eils. 2014. Dissecting the contribution of actin and vimentin intermediate filaments to mechanical phenotype of suspended cells using high-throughput deformability measurements and computational modeling. *J. Biomech.* 47:2598–2605.
10. Wang, N., and D. Stamenović. 2000. Contribution of intermediate filaments to cell stiffness, stiffening, and growth. *Am. J. Physiol. Cell Physiol.* 279:C188–C194.
11. Clemen, C. S., H. Herrmann, …, R. Schröder. 2013. Desminopathies: pathology and mechanisms. *Acta Neuropathol.* 125:47–75.
12. De Bleecker, J. L., A. G. Engel, and B. B. Ertl. 1996. Myofibrillar myopathy with abnormal foci of desmin positivity. II. Immunocytochemical analysis reveals accumulation of multiple other proteins. *J. Neuropathol. Exp. Neurol.* 55:563–577.
13. Selcen, D., and A. G. Engel. 1993. Myofibrillar myopathy. *In* GeneReviews. R. A. Pagon, M. P. Adam, T. D. Bird, C. R. Dolan, C.-T. Fong, R. J. Smith, and K. Stephens, editors. University of Washington, Seattle, WA.
14. Bär, H., M. Schopferer, …, N. Willenbacher. 2010. Mutations in desmin's carboxy-terminal "tail" domain severely modify filament and network mechanics. *J. Mol. Biol.* 397:1188–1198.
15. Schopferer, M., H. Bär, …, N. Willenbacher. 2009. Desmin and vimentin intermediate filament networks: their viscoelastic properties investigated by mechanical rheometry. *J. Mol. Biol.* 388:133–143.
16. Bär, H., S. V. Strelkov, …, H. Herrmann. 2004. The biology of desmin filaments: how do mutations affect their structure, assembly, and organisation? *J. Struct. Biol.* 148:137–152.
17. Bär, H., N. Mücke, …, H. Herrmann. 2005. Severe muscle disease-causing desmin mutations interfere with in vitro filament assembly at distinct stages. *Proc. Natl. Acad. Sci. USA.* 102:15099–15104.
18. Joanne, P., O. Chourbagi, …, O. Agbulut. 2013. Viral-mediated expression of desmin mutants to create mouse models of myofibrillar myopathy. *Skelet. Muscle.* 3:4.

19. Capetanaki, Y., D. J. Milner, and G. Weitzer. 1997. Desmin in muscle formation and maintenance: knockouts and consequences. *Cell Struct. Funct.* 22:103–116.

20. Kreplak, L., and H. Bär. 2009. Severe myopathy mutations modify the nanomechanics of desmin intermediate filaments. *J. Mol. Biol.* 385:1043–1051.

21. Plodinec, M., M. Loparic, …, C.-A. Schoenenberger. 2011. The nanomechanical properties of rat fibroblasts are modulated by interfering with the vimentin intermediate filament system. *J. Struct. Biol.* 174:476–484.

22. Bonakdar, N., J. Luczak, …, B. Fabry. 2012. Biomechanical characterization of a desminopathy in primary human myoblasts. *Biochem. Biophys. Res. Commun.* 419:703–707.

23. Leccia, E., S. Batonnet-Pichon, …, F. Briki. 2013. Cyclic stretch reveals a mechanical role for intermediate filaments in a desminopathic cell model. *Phys. Biol.* 10:016001–016009.

24. Pruszczyk, P., A. Kostera-Pruszczyk, …, A. Kamińska. 2007. Restrictive cardiomyopathy with atrioventricular conduction block resulting from a desmin mutation. *Int. J. Cardiol.* 117:244–253.

25. Goudeau, B., F. Rodrigues-Lima, …, P. Vicart. 2006. Variable pathogenic potentials of mutations located in the desmin alpha-helical domain. *Hum. Mutat.* 27:906–913.

26. Segard, B.-D., F. Delort, …, S. Batonnet-Pichon. 2013. *N*-acetyl-L-cysteine prevents stress-induced desmin aggregation in cellular models of desminopathy. *PLoS One.* 8:e76361.

27. Bureau, L., and M. Balland. 2014. Thermosensitive micropatterned substrates. *Methods Cell Biol.* 120:145–154.

28. Schindelin, J., I. Arganda-Carreras, …, A. Cardona. 2012. Fiji: an open-source platform for biological-image analysis. *Nat. Methods.* 9:676–682.

29. Zemel, A., F. Rehfeldt, …, S. A. Safran. 2010. Optimal matrix rigidity for stress fiber polarization in stem cells. *Nat. Phys.* 6:468–473.

30. Desprat, N., A. Richert, …, A. Asnacios. 2005. Creep function of a single living cell. *Biophys. J.* 88:2224–2233.

31. Desprat, N., A. Guiroy, and A. Asnacios. 2006. Microplates-based rheometer for a single living cell. *Rev. Sci. Instrum.* 77:055111.

32. Mitrossilis, D., J. Fouchard, …, A. Asnacios. 2009. Single-cell response to stiffness exhibits muscle-like behavior. *Proc. Natl. Acad. Sci. USA.* 106:18243–18248.

33. Fouchard, J., C. Bimbard, …, A. Asnacios. 2014. Three-dimensional cell body shape dictates the onset of traction force generation and growth of focal adhesions. *Proc. Natl. Acad. Sci. USA.* 111:13075–13080.

34. Mitrossilis, D., J. Fouchard, …, A. Asnacios. 2010. Real-time single-cell response to stiffness. *Proc. Natl. Acad. Sci. USA.* 107:16518–16523.

35. Tseng, Q., I. Wang, …, M. Balland. 2011. A new micropatterning method of soft substrates reveals that different tumorigenic signals can promote or reduce cell contraction levels. *Lab Chip.* 11:2231–2240.

36. Butler, J. P., I. M. Tolić-Nørrelykke, …, J. J. Fredberg. 2002. Traction fields, moments, and strain energy that cells exert on their surroundings. *Am. J. Physiol. Cell Physiol.* 282:C595–C605.

37. Sabass, B., M. L. Gardel, …, U. S. Schwarz. 2008. High resolution traction force microscopy based on experimental and computational advances. *Biophys. J.* 94:207–220.

38. Fabry, B., G. N. Maksym, …, J. J. Fredberg. 2001. Scaling the microrheology of living cells. *Phys. Rev. Lett.* 87:148102-1–148102-4.

39. Balland, M., N. Desprat, …, F. Gallet. 2006. Power laws in microrheology experiments on living cells: Comparative analysis and modeling. *Phys. Rev. E Stat. Nonlin. Soft Matter Phys.* 74:021911.

40. Icard-Arcizet, D., O. Cardoso, …, S. Hénon. 2008. Cell stiffening in response to external stress is correlated to actin recruitment. *Biophys. J.* 94:2906–2913.

41. Bär, H., B. Goudeau, …, H. Herrmann. 2007. Conspicuous involvement of desmin tail mutations in diverse cardiac and skeletal myopathies. *Hum. Mutat.* 28:374–386.

42. Herrmann, H., S. V. Strelkov, …, U. Aebi. 2000. The intermediate filament protein consensus motif of helix 2B: its atomic structure and contribution to assembly. *J. Mol. Biol.* 298:817–832.

43. Dupin, I., Y. Sakamoto, and S. Etienne-Manneville. 2011. Cytoplasmic intermediate filaments mediate actin-driven positioning of the nucleus. *J. Cell Sci.* 124:865–872.

44. Seifert, G. J., D. Lawson, and G. Wiche. 1992. Immunolocalization of the intermediate filament-associated protein plectin at focal contacts and actin stress fibers. *Eur. J. Cell Biol.* 59:138–147.

45. Dasbiswas, K., S. Majkut, …, S. A. Safran. 2015. Substrate stiffness-modulated registry phase correlations in cardiomyocytes map structural order to coherent beating. *Nat. Commun.* 6:6085.